Insights into Super-stable Mineralization of Cr(III) from Wastewater by CuO

Jiaxin Li,[a] Tianyang Shen,[a] Huijuan Wang,[a] Shaoquan Li,[a] Jikang Wang,[a] Gareth R. Williams,[b] Yufei Zhao,*[a] Xianggui Kong,[a] Lirong Zheng[c] and Yu-Fei Song*[a]

[a]State Key Laboratory of Chemical Resource Engineering, Beijing University of Chemical Technology, Beijing 100029 P. R. China. E-mail: songyf@mail.buct.edu.cn; Tel/Fax: +86-10-64431832.

[b]UCL School of Pharmacy, University College London, 29–39 Brunswick Square, London, WC1N 1AX, UK

[c]Beijing Synchrotron Radiation Facility Institute of High Energy Physics, Chinese Academy of Sciences, Beijing 100049, China.

ABSTRACT: The removal of Cr(III) ions from contaminated wastewater is of great urgency both from environmental protection and resource utilization perspectives. Herein, we developed a super-stable mineralization method to immobilize Cr^{3+} ions from wastewater using CuO as a stabilizer, leading to the formation of CuCr-layered double hydroxide (denoted as CuCr-LDH). The CuO showed superior Cr^{3+} removal performance with the removal efficiency of 97.97% and the maximum adsorption capacity of 207.6 mg/g in 13000 mg/L Cr^{3+} ions solution. *In situ* and *ex situ* X-ray absorption fine structure (XAFS) characterizations were carried out to elucidate the super-stable mineralization mechanism. Two reaction pathways were proposed including coprecipitation-dissolution and topological transformation. The mineralized product of CuCr-LDH can be reused for removing organic dyes efficiently, and the adsorption capacities were up to 248.0 $mg \cdot g^{-1}$ for Congo red and 240.1 $mg \cdot g^{-1}$ for Evans blue, respectively. Moreover, the CuCr-LDH exhibited good performance for photocatalytic CO_2 reduction to syngas (H_2/CO=2.66) with the evolution rate of CO of 54.03 $\mu mol \cdot g^{-1} \cdot h^{-1}$ and H_2 of 143.94 $\mu mol \cdot g^{-1} \cdot h^{-1}$ under λ >400 nm, respectively. More encouragingly, the actual tanning leather Cr^{3+} wastewater treated by CuO showed that the Cr^{3+} can reduce from 3438 mg/L to 0.06 mg/L, which was much below discharge standards (1.5 mg/L). This work provides a new approach to mineralization of Cr^{3+} ions through the "salt-oxide" route and the findings reported herein may guide the future design of highly efficient mineralization agents for heavy metals.

Keywords: Cr^{3+} ions, Layered double hydroxide, Super-stable mineralization, Reutilization, Photocatalytic CO_2 reduction

1. INTRODUCTION

Heavy metal ions, such as chromium (Cr), are widely used at high levels in industries such as leather tanning, electroplating, textiles and metallurgy.[1, 2] The trivalent Cr(III) and hexavalent Cr(VI) ions are often present in wastewater,[3, 4] and Cr(VI) is much more toxic than Cr(III).[5] It is well known that the Cr(VI) ions can be reduced to Cr(III) by adding Fe(II) salts or other reducing agents,[6, 7] and the Cr(III) ions can easily be re-oxidized back to Cr(VI).[8, 9] Therefore, it is vital to develop green and effective technologies for removing Cr ions from contaminated wastewater. Many methods, including chelating,[10] membrane separation,[11] ion exchange,[12] electrochemical treatment,[13] chemical precipitation[4, 14] and adsorption,[15] have been widely used to remove Cr ions. For example, Saleh *et al.* synthesized a cross-linked tetrapolymeric anionic polyelectrolyte (CAPE) with multiple functionalities, which showed good removal performance for Cr^{3+} by chelation interaction.[10] Gao et al. reported a membrane separation method using PANI@PS (PANI = polyaniline; PS = polystyrene balls) composites as adsorbents to immobilize Cr^{3+} through the confinement effects in polymers.[11] However, the chelation and membrane separation methods were largely restricted by the low efficiency and time-consuming. In addition, ion exchange and electrochemical treatment methods showed disadvantages such as the high cost and energy consumption *etc*.[16] In industry, a chemical precipitation method using lime or other alkali sources is usually applied to convert Cr^{3+} ions in wastewater to $Cr(OH)_3$ sludge.[4, 14] However, the lime precipitation method requires a large amount of alkaline solution with a high pH value (pH = 9-11).[17, 18] Moreover, these useless solid sludge

and wastewater commonly need further treatment to meet with the waste discharge limit.[5, 19] Therefore, green and clean procedure for efficient removal of Cr^{3+} ions from wastewater is of great urgency.

Layered double hydroxides (LDHs), a kind of inorganic layered matrices, have attracted great research interest for environmental and other applications.[20-26] The general formula of LDHs is $[M(II)_{1-x}M(III)_x(OH)_2]^{x+}$ $[A_{x/n}\ H_2O]^{x-}$, with M(II) and M(III) representing metallic cations (e.g. Zn^{2+}, Ni^{2+}, Co^{3+}, Fe^{3+}, Cr^{3+}, Cu^{2+}, *etc*), while A denotes an interlayer anion.[27-31] LDHs can be used as adsorbents for removal of hazardous anions (F^-, CrO_4^{2-} and $HAsO_4^{2-}$) [32-34] by the ion-exchange properties and removal of heavy metal cations (Cd^{2+}, Ni^{2+} and Zn^{2+}) through the isomorphous substitution[17, 26, 35] or chelation process.[36] The K_{sp} of Cr^{3+}-containing LDH (~10^{-62}) is significantly lower than that of $Cr(OH)_3$ (~10^{-31}), suggesting that Cr^{3+} ions can be effectively mineralized when the Cr^{3+} ions are introduced into the LDH.[37] Therefore, mineralization through introducing Cr^{3+} ions into LDHs shows tremendous potential for reducing the solubility and mobility of these harmful heavy metal ions. Recently, the "salt-oxide" route, which involves LDH synthesis *via* a direct reaction between a metal salt solution and a metal oxide or hydroxide, has aroused great attention as a clean and simple process without further addition of alkali solution.[38-40] CuO, as an inexpensive electronic residue, is considered a promising precursor to form Cu-based LDHs with low K_{sp}.[39, 41, 42] Therefore, we adopt CuO to treat with Cr^{3+} wastewater, which results in the formation of the super-stable structure of LDH *via* the "salt-oxide" route.

Herein, we reported the use of CuO nanoparticles as a stabilizer to remove Cr^{3+} ions from wastewater, which resulted in the formation of the super-stable mineralization structure of CuCr-LDH *via* the "salt-oxide" route (Scheme 1). X-ray diffraction (XRD), high-resolution transmission electron microscopy (HRTEM), *in situ* and *ex situ* XAFS were adopted to reveal the mineralization mechanism of Cr(III) ions by CuO. A systematic investigation of the use of CuCr-LDH for removing organic dyes and photocatalytic CO_2 reduction to syngas was carried out.

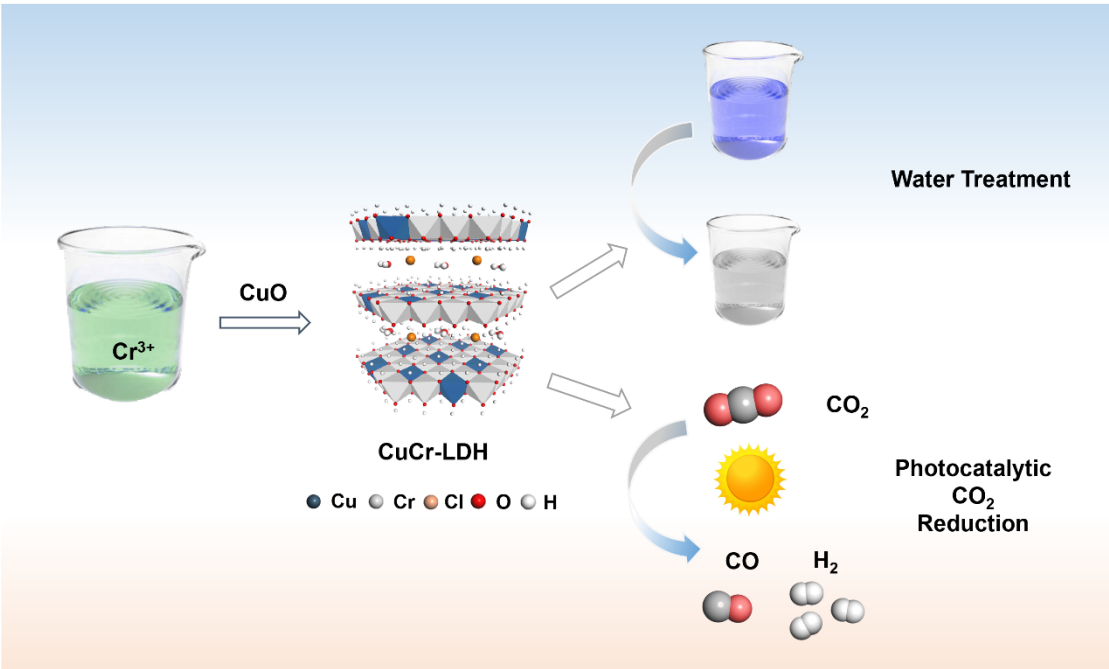

Scheme 1. Schematic illustrating the process of super-stable mineralizing Cr(III) ions from wastewater using CuO as the stabilizer and the use of the mineralized product (CuCr-LDH) to remove organic dyes and photocatalytic CO_2 reduction.

2. RESULTS AND DISCUSSION

2.1. Super-stable Mineralization of Cr^{3+} Using CuO.

In this study, we used CuO as a stabilizer to remove Cr^{3+} ions from solution using

the “salt-oxide” route. After adding the CuO into Cr^{3+} ions solution, the precipitate was recovered by centrifugation. As expected, the precipitate showed typical XRD diffractions of (003), (006), (012), (110) and (113), indicating the formation of CuCr-LDH (Figure 1a).[43] The CuO exhibited granular morphology with an average particle diameter of ~82 nm (Figure S1a-b). In contrast, the CuCr-LDH showed large sheets with a diameter of 1~2 μm and thickness of ~491 nm (Figure S1c-d). In addition, energy dispersive spectroscopy (EDS) mapping results of the formed CuCr-LDH showed that Cu, Cr, O and Cl were uniformly dispersed, which suggested that a Cl^- intercalated LDH was produced (Figure S1e-f). Furthermore, the inductively-coupled plasma optical-emission spectrometry (ICP-OES) displayed that the value of atomic ratios of Cu/Cr was 2.19 (Table S1), which was consistent with the stoichiometric ratio of $Cu_{0.67}Cr_{0.33}(OH)_2Cl_{0.33}\cdot xH_2O$ (JCPDS 51–0161). In addition, the interference of solution pH, coexisted inorganic ions and organic matters was also investigated. It was found that these factors showed an insignificant impact on the formation of CuCr-LDH structure (Figure S2). These results indicated that CuO can mineralize the Cr^{3+} ions, leading to the formation of CuCr-LDH with good anti-interference ability.

Furthermore, we evaluated the removal capability of Cr^{3+} ions using CuO as a stabilizer. As shown in Figure 1b, when the initial concentration of Cr^{3+} was 13000 mg/L in the presence of 0.02 mol CuO, the removal efficiency of ~55.81% can be achieved after 10 h. Further increasing the CuO amount to 0.04 mol, the removal efficiency reached 97.97%. Similarly, 99.92% of removal efficiency can be obtained at a markedly lower Cr^{3+} concentration (1625 mg/L) when using 0.0050 mol CuO (Figure

S3a and Table S2). Additionally, the adsorption kinetics of Cr^{3+} ions using CuO as a stabilizer were further investigated. As displayed in Table S3, log (q_e-q_t) as a function of time (t) was not well consistent with pseudo-first-order kinetic model with poor correlations (R^2 = 0.8515) (C_0= 13000 mg/L, dose = 0.04 mol). Conversely, t/q_t as a function of time (t) was more in line with the pseudo-second-order kinetic model with R^2 = 0.9978 (Figure 1c). Similarly, the adsorption manner was well-matched with the pseudo-second-order kinetic model when the initial concentration of Cr^{3+} was 1625 mg/L (Figure S3b and Table S3). These results suggested that the adsorption process towards Cr^{3+} ions by CuO was essentially controlled by chemical adsorption rather than mass transport.[44] As shown in Figure S4, the maximum saturated Cr^{3+} adsorption capacity of CuO can reach 207.6 mg/g, which was higher than most reported sorbents (Table S4). Additionally, the adsorption isotherm of Cr^{3+} ions was well fitted well into the Langmuir model with R^2 = 0.9994 (Figure 1d and Table S5).[26] Furthermore, the removal of actual Cr^{3+} contaminated tanning leather wastewater from a tannery in Hebei, China by using CuO was carried out. As shown in Figure S5 and Table S6, after treatment by CuO for 48 h at 35 °C, the concentration of Cr^{3+} was significantly reduced from 3438 to 0.06 mg/L, which was much below the discharge standard limit (GB 30486-2013, total Cr: 1.5 mg/L).[45, 46] Based on the above results, it can be reasonably concluded that CuO was an efficient mineralization stabilizer for the removal of Cr^{3+} ions from wastewater.

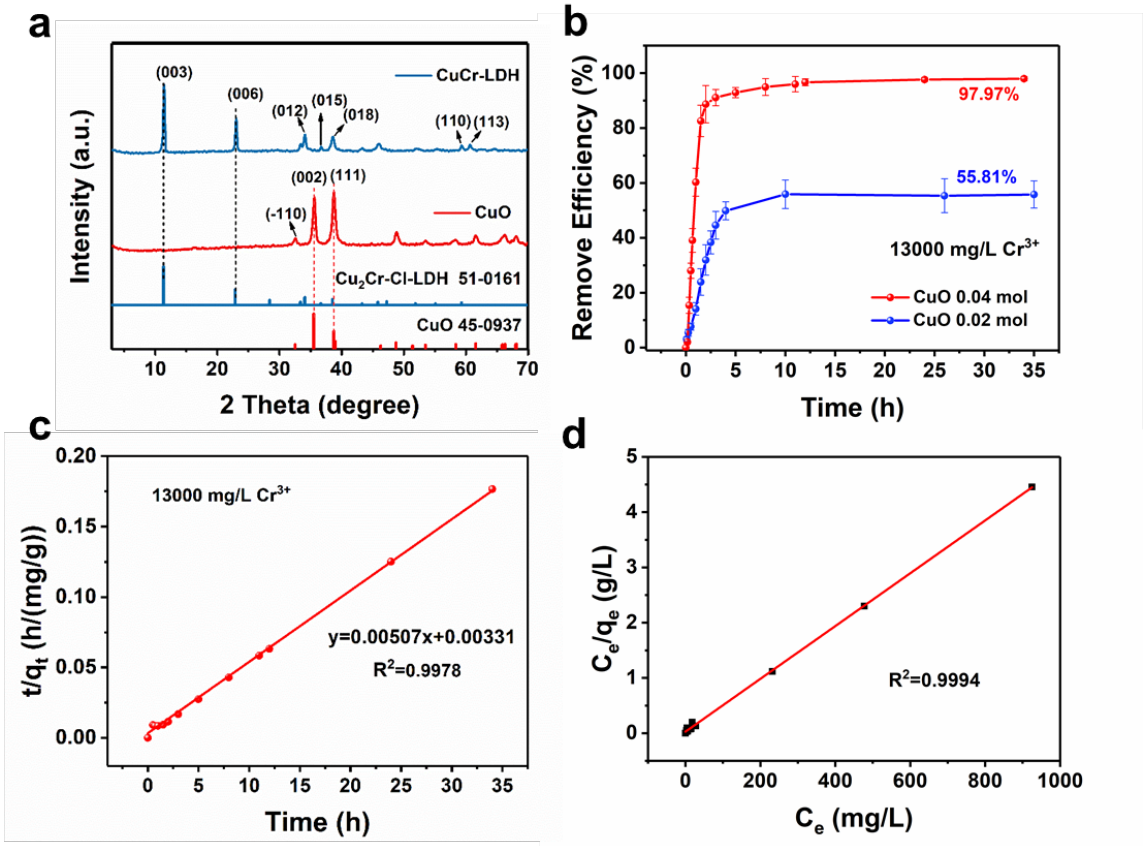

Figure 1. (a) X-ray diffraction (XRD) patterns of the mineralized product (CuCr-LDH) recovered after removing Cr^{3+} using CuO for 34 h (Condition: CuO = 0.02 mol, C_0 = 13000 mg/L, V = 40 mL, 34 h, 35 °C); (b) the removal percentage of Cr^{3+} using CuO as stabilizer; (c) the fitting plot of pseudo-second-order kinetic models from Cr^{3+} adsorption (Condition: CuO = 0.02 or 0.04 mol, C_0 = 13000 mg/L, V = 40 mL, t = 0-34 h, 35 °C); (d) the fitting plot of Langmuir model from Cr^{3+} adsorption.

2.2. Mechanistic Studies of Super-stable Mineralization of Cr^{3+}.

XRD patterns were performed to explore the structural and compositional change of CuO. As shown in Figure S6, XRD pattern of CuO showed a decrease with increase of the mineralization time. The characteristic (003) and (006) basal peaks of LDH can be observed in 0.5 h, and the diffraction peak for CuO disappeared completely after 6 h

and the CuO was converted to the corresponding CuCr-LDH. During the mineralization process in 6 h, visible color changes from black to gray-green can be observed obviously (Figure S7a) and the pH of the reaction system increased gradually from 2.74 to 3.40 (Figure S7b). Moreover, SEM images showed that large plates started to appear in 0.5 h (Figure S8a-b) and the original particles were transformed completely into the plates with a thickness of 400-457 nm in 6 h, which corresponded to the conversion of CuO particles to the CuCr-LDH plates (Figure S8c-f). Transmission electron microscopy (TEM) images exhibited a similar transformation from CuO particles to large sheets of CuCr-LDH in 6 h (Figure S9a-d)

HRTEM images showed that the dominated particles at 0.5 h exhibited an interplanar spacing of 0.250 nm, which was assigned to the (002) plane of CuO (Figure S10a-b). Interestingly, small hexagonal platelets with a diameter of ~3 nm and lattice space of 0.240 nm can be observed around CuO particles (Figure 2a-b), which can be attributed to the (015) plane of CuCr-LDH. The results indicated that the solid CuO released some Cu^{2+} ions at acid pH to drive the formation of the CuCr-LDH phase through a dissolution-reprecipitation route, which was consistent with the results previously reported.[39]

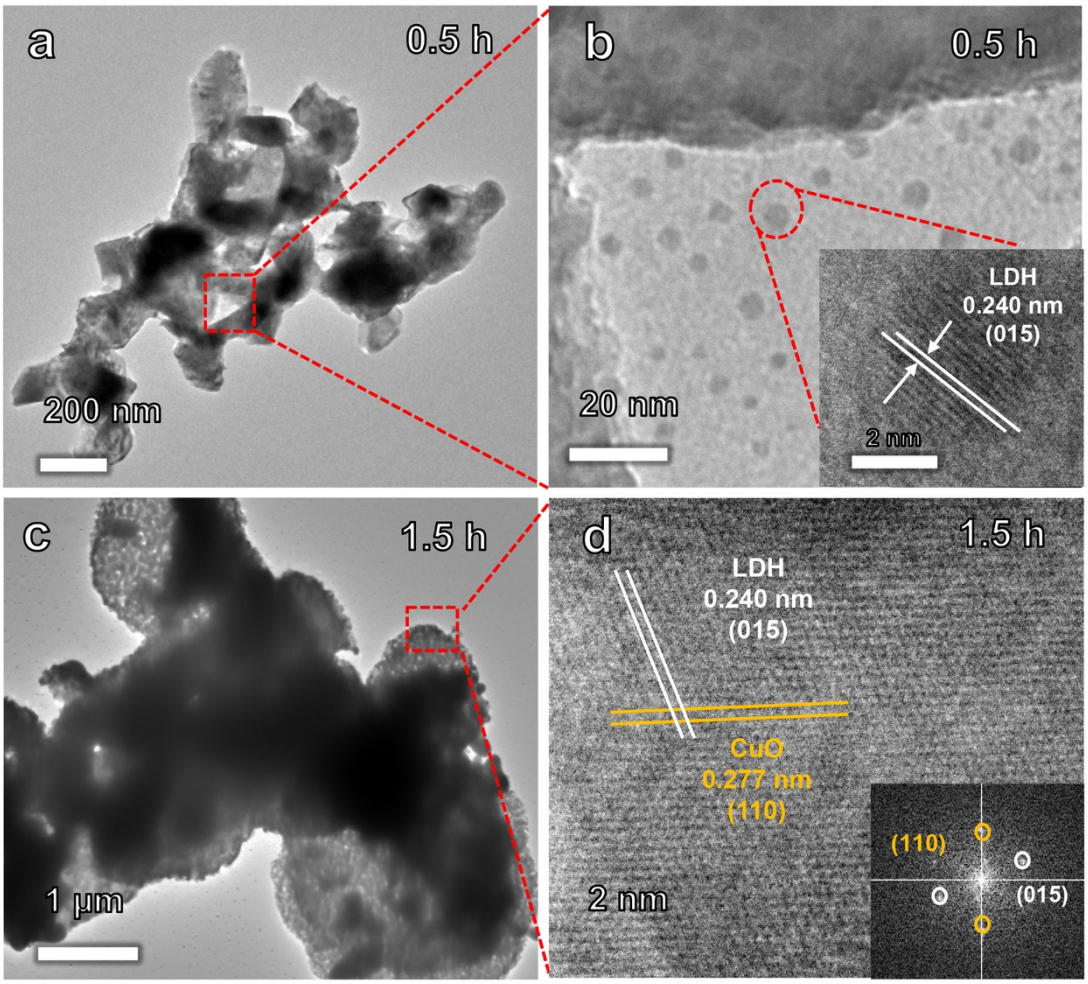

Figure 2. TEM and HRTEM images of the mineralization process at different times: 0.5 h (a and b), 1.5 h (c), 3 h (c) and 6 h (d). (dose = 0.02 mol, C_0 [Cr^{3+}] = 13000 mg/L, V = 40 mL, t = 0-34 h, 35 °C)

Contrast experiments using $CuCl_2$ as a precursor showed that CuCr-LDH can be formed at weakly acidic pH by the co-precipitation route (Figure S9e-f). As shown in Figure S9g-h, it should be noted that the size of the formed CuCr-LDH by the co-precipitation method was around 11 nm, which was much smaller than that of CuCr-LDH synthesized by the "salt-oxide" method (1~2 μm) (Figure S9d). The results indicated that there may be other pathways for the transformation of CuO to CuCr-LDH during the mineralization process of Cr^{3+} ion. It can be seen that when the

mineralization time was 1.5 h, the large sheet was made up of many particles with the size of ~60 nm spliced together (Figure 2c and Figure S10c). Furthermore, the lattice fringes of these particles were found to be 0.277 and 0.240 nm, corresponding to the (110) plane of CuO and (015) plane of CuCr-LDH, respectively (Figure 2d). After mineralization for 3 h, only a few particles were left on the large sheets (Figure S10d), and the small particles disappeared completely in 6 h and solely large and thick hexagonal sheets can be observed (Figure S10e), which can be demonstrated to be the CuCr-LDH based on the corresponding lattice fringe and FFT pattern (Figure S10f).[47] The co-existence of CuO particles and newly formed CuCr-LDH sheets indicated that a topological transformation process may take place during the mineralization of Cr^{3+} ions.

2.3. Mechanism studies using XAFS Analysis.

With the aim of exploring the phase transformation from CuO to LDH and the underlying mechanisms, XAFS spectra were performed to reveal the coordination environment and electronic structures in the mineralized products.[48] As displayed in Figure 3a, the Cu K-edge absorption positions of the mineralized products at different mineralization times (t = 0.5, 1.5, 3, 6, 10 h) and CuCr-LDH were nearly the same as that of CuO, suggesting the +2 oxidation state of Cu^{2+} in all samples. In addition, a broad pre-edge peak at ~8985 eV in CuO can be observed, which was attributed to the four-coordinate geometry of Cu^{2+} ions.[49] This peak decreased gradually with increase of the mineralization time from 0.5 to 10 h, which indicated the coordination symmetry

of Cu^{2+} ions changed to from tetrahedron to octahedral geometry. From the *k*-space plot (Figure 3b), the oscillation spectra of collected products at the mineralization time of 0.5 h and 1.5 h were similar to CuO, indicating CuO was the dominant component in the products. However, the *k*-space spectrum of the solid product at the mineralization time of 3 h showed different oscillation positions at 4.6 $Å^{-1}$ and 6.5 $Å^{-1}$ when compared with CuO, which was very much similar to CuCr-LDH. This result indicated that most CuO was converted to the corresponding LDH structure.[50] Figure 3c depicted the R-space plots of CuO and the mineralized products at different mineralization times (t=0.5, 1.5, 3, 6, 10 h). It was evident that CuO exhibited three characteristic peaks (Figure 3c), in which Peak A represented the first Cu-O shell, while peak B and peak C corresponded to the second Cu-O-Cu1 shell and the third Cu-O-Cu2 shell, respectively (Figure S11).[51, 52] As shown in Table S7 and Figure S12, the coordination number (*N*) of Cu-O shell at ~1.50 Å increased from 4.0 to 6.0, indicating that the geometry of four coordination of CuO_4 was converted to octahedron geometry of six coordination of CuO_6 in CuCr-LDH. In contrast, the *N* of Cu-O-Cu1 shell (peak B) decreased gradually from 4.0 (CuO) to 1.2 (3 h), suggesting that the Cu1 atoms in Cu-O-Cu1 shell for CuO structure was released during the mineralization process of Cr^{3+} ions. In addition, FT-EXAFS spectra collected at mineralization time of 6 h and 10 h exhibited a new peak (peak D) at ~2.75 Å, which can be assigned to be the second Cu-O-M shell (M = Cu or Cr) of CuCr-LDH (Figure 3c and Figure S11-12). The increased coordination number of Cu-O-M after 3 h implied that the Cr^{3+} ions were trapped into the laminates of CuCr-LDH gradually (Table S7).

Wavelet transform (WT) analysis can facilitate the identification of the backscattering atom and provide both resolutions in radial distance *k*-space of the Cu K-edge EXAFS data, which can be used to demonstrate the structure changes during the mineralization of Cr^{3+} ions.[29] As shown in the wavelet transforms (WT) plots (Figure S13), there were two intensity maximum regions around $1 < (R + \alpha) < 2$ Å and $2 < (R + \alpha) < 3$ Å, which can be corresponded to the Cu-O shell and Cu-O-X shell (M=Cu or Cr) in the CuO and CuCr-LDH, respectively. It can be observed that there was no distinctive change in the first Cu-O shell, illustrating that the Cu-O bond distance remained unchanged throughout the topological transformation process. However, the coordination environment of the second shell (Cu-O-X) changed greatly. This change can be divided into two stages. In the first stage from the beginning to 1.5 h, the location of intensity maximum decreased to 3.9 $Å^{-1}$, indicating that the Cu1 atoms in the Cu-O-Cu1 shell of CuO structure were reducing gradually (Figure 3d and Figure S13), which was in good line with the results of R space (Figure 3c). On the contrary, in the second stage after 3h, the location of the second shell increased from 5.0 $Å^{-1}$ (3 h) to 5.5 $Å^{-1}$ (CuCr-LDH), which suggested that this stage was dominated by the mineralization of Cr atoms into the second shell of CuCr-LDH (Figure 3d).

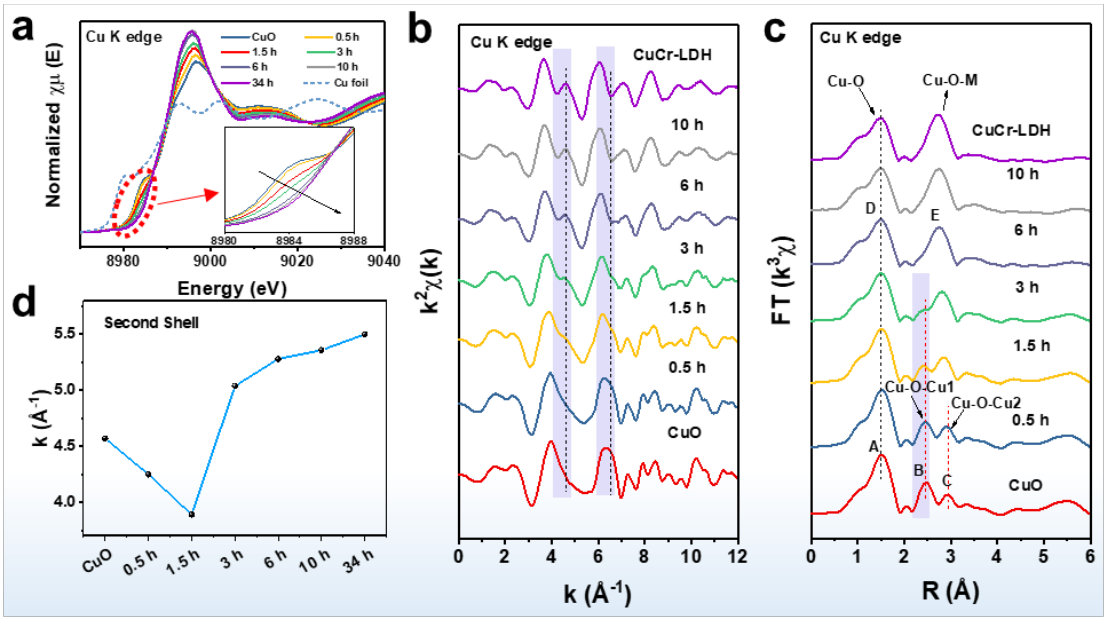

Figure 3. (a) X-ray absorption near edge structure (XANES) at Cu K-edge; (b) the oscillation function $k^2\chi(k)$ of the K-edge for Cu in the EXAFS; (c) the magnitude of weighted FT of Cu K-edge EXAFS; (d) the x-value of wavelet transforms signals for CuO, the mineralized products at different mineralization times (t=0.5, 1.5, 3, 6, 10 h) and CuCr-LDH.

For Cr K-edge XAFS spectra, the absorption positions of the mineralized products at different times were nearly the same as $Cr(OH)_3$, indicating the Cr atoms in these samples possessed the +3 oxidation state (Figure S14a-b).[47] And the *k* and R-space plots of the mineralized products at different times were close to the CuCr-LDH product (Figure S14c-d). EXAFS fitting of Cr^{3+} showed that the distance of Cr-O-Cu shell of the mineralized products at different times was much similar to that of CuCr-LDH (Figure S15 and Table S8). These results demonstrated that CuO in the presence of Cr^{3+} solution was transformed to CuCr-LDH. In addition, the ICP-OES (Table S9) showed that the Cu/Cr molar ratio decreased gradually and finally approached 2:1, indicating that CuO was gradually transformed into CuCr-LDH with the increase of the

mineralization time. To further confirm the local structure during the transformation from CuO to LDH, *in situ* XAFS measurements at the Cu and Cr K-edges were carried out (Figure S16). The results demonstrated that the trend of pre-edge features was similar to *ex situ* XAFS spectra, confirming the transformation from CuO to CuCr-LDH during mineralization of Cr^{3+} ion (Figure S17-18).

On the basis of the above results, insight into the mineralization process of Cr^{3+} ions by CuO can be summarized into two pathways, that is, dissolution-reprecipitation and topological transformation (Figure 4). On the one hand, CuO was partially dissolved in a weakly acidic solution,[39] and the released Cu^{2+} ions triggered a coprecipitation reaction in the presence of Cr^{3+} ions, Cl^- ions and H_2O, leading to the formation of CuCr-LDH due to the extremely low Ksp. On the other hand, the CuCr-LDH can be formed through the topological transformation from CuO, in which the Cu1 atoms in Cu-O-Cu1 (the second shell) of CuO were released preferentially under a weakly acidic condition. And then the neighboring O1 atom was exposed to coordinate with the central Cu atom. Finally, the configuration transformation took place, resulting in the formation of a six-coordinate CuO_6 octahedral structure in CuCr-LDH.

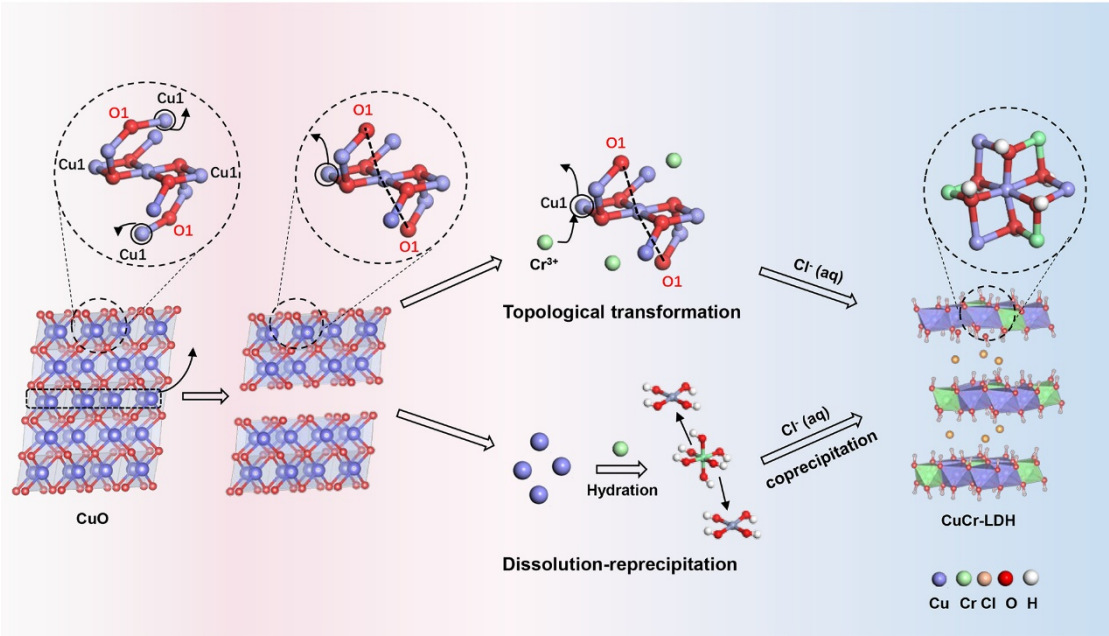

Figure 4. Schematic illustrating the proposed mechanisms of generating CuCr-LDH from CuO and aqueous Cr^{3+} ions.

2.4. Adsorption Tests and Photocatalytic CO_2 Reduction.

LDHs, being composed of positively charged laminate and negatively charged intercalated anions, can be used as adsorbents to remove anionic dyes from wastewater.[53, 54] To evaluate the adsorption ability of the mineralized product of CuCr-LDH for the removal of anionic dyes like Congo red (CR) and Evans blue (EB) (Figure S19a), 20 mg CuCr-LDH was added to 50 mL of EB and CR solutions (20 mg L^{-1}). As shown in Figure 5, EB and CR dye can be completely removed by CuCr-LDH in 260 min and 30 min, respectively. The maximum capacities of CuCr-LDH for EB and CR were found to be 240.1 and 248.0 mg/g, respectively (Figure S19b-c), much higher than that of CuO (giving a capacity < 20 mg g^{-1} for EB, < 30 mg g^{-1} for CR) (Figure S20), which was attributed to the much more positive surface charge of CuCr-LDH (+80.0 mV) than CuO (+12.8 mV) (Figure S21).[55] Both adsorptions followed a pseudo-second-

order model (Table S10), suggesting a chemisorption process onto CuCr-LDH and CuO (Figure 5c-d and Figure S20).[56] Moreover, the CuCr-LDH exhibited much better adsorption capacity for EB and CR pollutants than carbons, metal oxides and other LDHs adsorbents (Table S11). FTIR spectra of the CuCr-LDH after dye adsorption showed new bands at 1040 and 1170 cm^{-1} (Figure S22a), which were attributed to S-O and S=O vibrations of EB (or CR).[57] And the XRD of CuCr-LDH were almost unchanged before and after adsorption of dyes (Figure S22b). Thus, we can conclude that the CR and EB were adsorbed on the surface of CuCr-LDH through electrostatic interaction.[58] These results proved that the mineralization product (CuCr-LDH) can be used as a promising candidate for removal of anionic organic dyes.

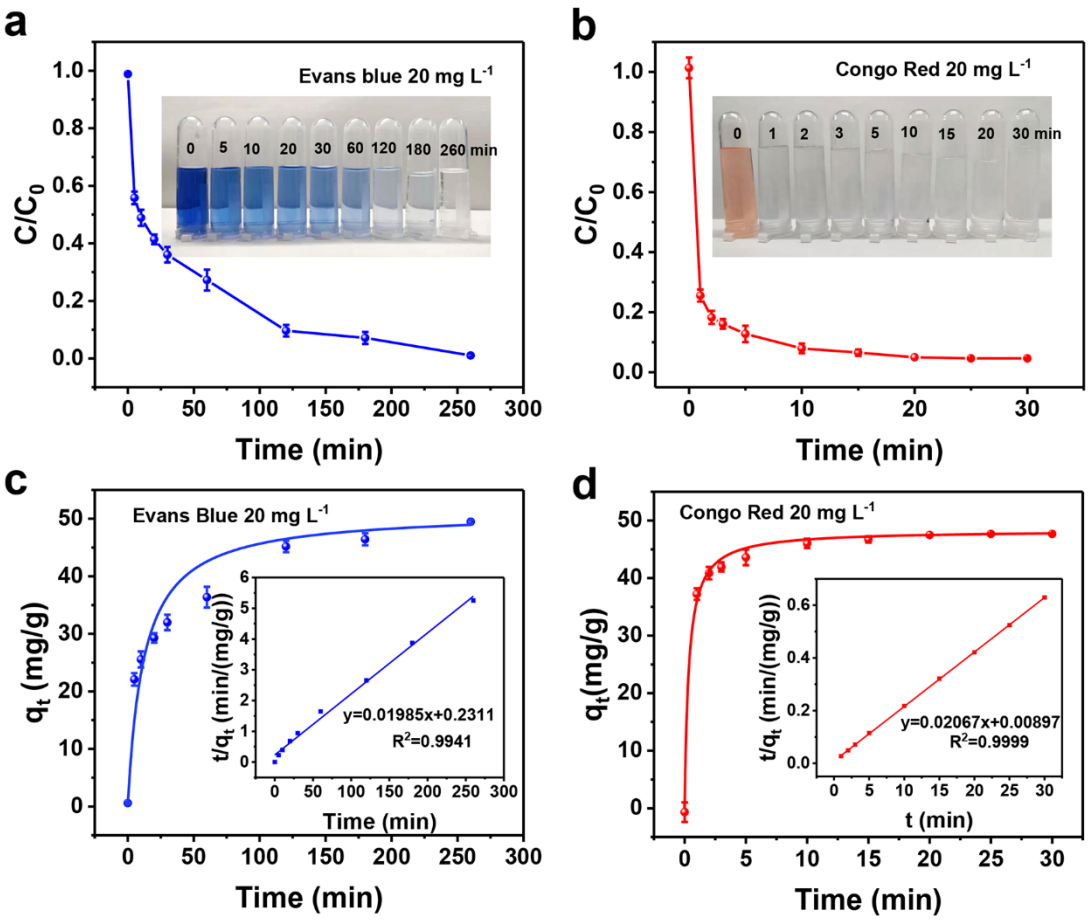

Figure 5. (a-b) The adsorption rates of CuCr-LDH (20 mg) towards EB and CR (20 mg L^{-1}, 50

mL); inset: the comparative photographs after different adsorption times. (c-d) Effect of the contact time on the adsorption of EB and CR onto CuCr-LDH. Inset: pseudo-second-order kinetic curves fitted by linear regression.

Recently, the solar-driven photocatalytic CO_2 conversion was a promising strategy for CO_2 utilization owing to its mild conditions.[59, 60] However, CO_2 conversion to high-value-added chemicals such as CO and H_2 that can be used for Fischer–Tropsch synthesis is highly demanding and challenging.[61, 62] Herein, the mineralization product CuCr-LDH and CuO precursor were used for CO_2 photoreduction (CO_2PR) reaction under visible light irradiation. As shown in UV-Vis diffuse reflectance spectra (Figure S23), the CuCr-LDH displayed two absorption bands at 410 and 570 nm in the visible region, which can be ascribed to the d-d transition $^4A_{2g}(F)\rightarrow{}^4T_{1g}(F)$ and $^4A_{2g}(F)\rightarrow{}^4T_{2g}(F)$ of the CrO_6 octahedra, respectively.[47] It can be seen from Figure 6a-b that under visible light irradiation (λ > 400 nm),[63, 64] the CuCr-LDH gave a high evolution rate of CO of 54.03 $\mu mol\cdot g^{-1}\cdot h^{-1}$ and H_2 of 143.94 $\mu mol\cdot g^{-1}\cdot h^{-1}$, which can be comparable to the catalytic performance of previously reported photocatalysts toward CO_2PR (Table S12).[65, 66] Furthermore, the syngas ratio (H_2/CO) was 2.66, which was ideal for the Fischer-Tropsch reaction to produce high-value-added chemicals.[67] In contrast, CO_2PR by CuO exhibited no CO products with only a small amount of H_2. Control experiments demonstrated that the CO product originated from CO_2 (Table S13). In addition, the activity and selectivity of CuCr-LDH were well retained after 4 cycles (Figure 6c), demonstrating the chemical stability of CuCr-LDH. Interestingly, CuCr-LDH retained great CO_2PR activity at a long wavelength (λ > 500 nm) (Figure

6d and Figure S24). To further probe why CuCr-LDH was more favorable for CO_2PR to CO than CuO, the band structures of CuO and CuCr-LDH were investigated. According to the results of Mott-Schottky plots (Figure S25a-c), the conduction band (CB) of CuO and CuCr-LDH were about -0.49 and -0.61 V versus NHE (pH = 7). Compared with the potential for CO_2PR (-0.53 V), CuCr-LDH can drive such reduction from CO_2 to CO, whereas CuO cannot (Figure S25d).[68] Besides, the photoluminescence (PL) intensity of CuCr-LDH (Figure S25e) was lower than CuO, indicating that CuCr-LDH had a higher photogenerated electron-hole separation efficiency, and further facilitated CO_2 reduction to CO.[61] A proposed mechanism of CuCr-LDH for photocatalytic CO_2 reduction were displayed in Figure S26.

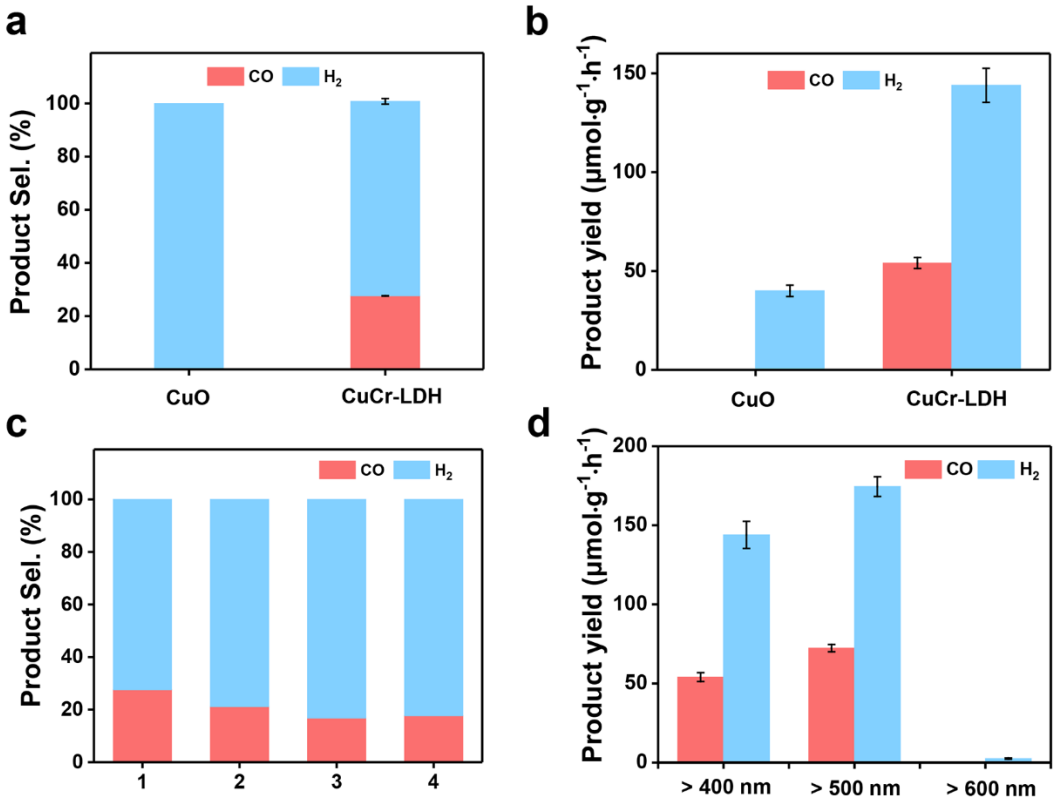

Figure 6. (a) Production selectivity and (b) rate of CO and H_2 for CuO and CuCr-LDH under λ >400 nm; (c) the recycle tests for CuCr-LDH; (d) the productivity of CO and H_2 on CuCr-

LDH under irradiation with different wavelength light (reaction condition: photocatalyst: 10 mg, photosensitizer: 4×10^{-6} mol $Ru(bpy)_3Cl_2 \cdot 6H_2O$, solvent: 10 mL H_2O/MeCN/TEOA (1:3:1, v/v/v); 1 h).

3. CONCLUSIONS

In summary, it was demonstrated herein that the Cr^{3+} ions can be effectively mineralized by CuO with a high mineralization capacity of 207.6 mg/g, resulting in the formation of CuCr-LDH. For the first time, *in situ* and *ex situ* XAFS analyses were applied to explore the Cr^{3+} mineralized mechanisms. It was proposed that the mineralization process involved two pathways. Firstly, CuO dissolved and the Cu^{2+} was released into solution. The combination of Cu^{2+}, Cr^{3+}, Cl^- and H_2O resulted in the formation of CuCr-LDH through the dissolution-reprecipitation. On the other hand, CuO can be *in situ* converted to CuCr-LDH *via* a topological transformation pathway, in which the planar geometry of four coordination of CuO_4 was transformed into octahedron geometry of six coordination of CuO_6, and CuCr-LDH was formed in the presence of $Cr^{3+}$and Cl^-. The mineralized product of CuCr-LDH showed fast adsorption rates and excellent adsorption capacities toward EB (248.0 mg/g) and CR (240.1 mg/g). In addition, the CuCr-LDH also displayed good performance of photocatalytic CO_2 reduction to syngas (H_2/CO=2.66) with the CO production rate (54.03 $\mu mol \cdot g^{-1} \cdot h^{-1}$) under visible light irradiation. More encouragingly, the treatment of the actual tanning leather wastewater sample by CuO showed that the Cr^{3+} can be reduced significantly from 3438 to 0.06 mg/L, which was much below the discharge standard limit (1.5 mg/L). This study demonstrates the super-stable mineralization of Cr^{3+} ions can be achieved

by using CuO and the resultant CuCr-LDH can be used for removal of organic dyes and photocatalytic CO_2 reduction.

ASSOCIATED CONTENT

Supporting Information.

SEM images, the performance of removing Cr^{3+} ions, FT-IR, XRD, TEM images, EXAFS analysis, *in situ* XAFS results, the removal performance of the EB and CR dyes by CuCr-LDH, the photocatalytic CO_2 reduction performance of CuCr-LDH. The Supporting Information is available free of charge on the ACS Publications website.

AUTHOR INFORMATION

Corresponding Author

*songyf@mail.buct.edu.cn;

Notes

The authors declare no competing financial interest.

ACKNOWLEDGMENTS

This research was supported by the National Nature Science Foundation of China (22178019, U1707603) and the Fundamental Research Funds for the Central Universities (XK1802-6, XK1803-05, XK1902, 12060093063). The XAFS experiments were conducted in 1W1B beamline of Beijing Synchrotron Radiation Facility (BSRF).

REFERENCES

(1) Qu, W.; He, D.; Guo, Y.; Tang, Y.; Shang, J.; Zhou, L.; Zhu, R.; Song, R.-J., Modified Water Hyacinth Functionalized with Citric Acid as an Effective and Inexpensive Adsorbent for Heavy Metal-Ion Removal. *Ind. Eng. Chem. Res.* **2019,** *58*, 18508-18518.

(2) Ruan, X.; Xu, Y.; Liao, X.; He, G.; Yan, X.; Dai, Y.; Zhang, N.; Du, L., Polyethyleneimine-Grafted Membranes for Simultaneously Adsorbing Heavy Metal Ions and Rejecting Suspended Particles in Wastewater. *AIChE J.* **2017,** *63*, 4541-4548.

(3) Li, Q.; Liu, Y.; Yu, X.; Li, L.; Zhang, X.; Lu, Z.; Lin, J.; Yang, X.; Huang, Y., Removal of Cr(III)/Cr(VI)from Wastewater Using Defective Porous Boron Nitride: A Dft Study. *Inorg. Chem. Front.* **2018,** *5*, 1933-1940.

(4) Sun, B.; Tian, H.-Y.; Zhang, C.-X.; An, G., Preparation of Biomimetic-Bone Materials and Their Application to the Removal of Heavy Metals. *AIChE J.* **2013,** *59*, 229-240.

(5) Li, W.-Q.; Liu, D.; Qu, J.-Y.; Luo, J.-H., Hydrothermal Synthesis of a Novel Nanolayered Tin Phosphate for Removing Cr(III). *RSC Adv.* **2021,** *11*, 3202-3208.

(6) Liu, L.-L.; Xing, Y.; Yu, H.-Y.; Zhang, C.-W.; Ye, M.-Q.; Miao, M.-Z.; Yu, C.-X., Effective Removal of Chromium(III) from Low Concentration Aqueous Solution Using a Novel Diazene/Methoxy-Laced Coordination Polymer. *Polymers* **2017,** *9*, 273-287.

(7) Luo, M. B.; Xiong, Y. Y.; Wu, H. Q.; Feng, X. F.; Li, J. Q.; Luo, F., The MOF^{+} Technique: A Significant Synergic Effect Enables High Performance Chromate Removal. *Angew. Chem. Int. Ed.* **2017,** *56*, 16376-16379.

(8) E, T.; Ma, D.; Yang, S.; Sun, Y.; Xu, J.; Kim, E. J., Zirconium Dioxide Loaded Montmorillonite Composites as High-Efficient Adsorbents for the Removal of Cr^{3+} Ions from Tanning Wastewater. *J. Solid State Chem.* **2019,** *277*, 502-509.

(9) Eyvazi, B.; Jamshidi-Zanjani, A.; Khodadadi Darban, A., Synthesis of Nano-Magnetic $MnFe_2O_4$ to Remove Cr(III) and Cr(VI) from Aqueous Solution: A Comprehensive Study. *Environ. Pollut. (Oxford, U. K.)* **2020,** *265*, 113685.

(10) Saleh, T. A.; Haladu, S. A.; Ali, S. A. A Novel Cross-Linked pH-Responsive Tetrapolymer: Synthesis, Characterization and Sorption Evaluation Towards Cr(III). *Chem. Eng. J.* **2015,** *269*, 9-19.

(11) Ding, J.; Pu, L.; Wang, Y.; Wu, B.; Yu, A.; Zhang, X.; Pan, B.; Zhang, Q.; Gao, G. Adsorption

and Reduction of Cr(VI) Together with Cr(III) Sequestration by Polyaniline Confined in Pores of Polystyrene Beads. *Environ. Sci. Technol.* **2018,** *52*, 12602-12611.

(12) Liang, R.; Han, L.; Wang, Y.; Wang, H.; Xiang, L.; Chen, S.; Lu, Q.; Yan, B. Novel Ti-Coordination Polydopamine Nanocomposite with a Combination of Adsorption, Reduction, and Ion Exchange for Rapid Cr(VI) Removal. *Ind. Eng. Chem. Res.* **2022,** *61*, 9717-9724.

(13) Su, X.; Kushima, A.; Halliday, C.; Zhou, J.; Li, J.; Hatton, T. A. Electrochemically-Mediated Selective Capture of Heavy Metal Chromium and Arsenic Oxyanions from Water. *Nat. Commun.* **2018,** *9*, 4701.

(14) Zhang, W.; Liu, F.; Sun, Y.; Zhang, J.; Hao, Z. Simultaneous Redox Conversion and Sequestration of Chromate(VI) and Arsenite(III) by Iron(III)-Alginate Based Photocatalysis. *Appl. Catal. B Environ.* **2019,** *259*, 118046.

(15) Lyu, W.; Wu, J.; Zhang, W.; Liu, Y.; Yu, M.; Zhao, Y.; Feng, J.; Yan, W., Easy Separated 3d Hierarchical Coral-Like Magnetic Polyaniline Adsorbent with Enhanced Performance in Adsorption and Reduction of Cr(VI) and Immobilization of Cr(III). *Chem. Eng. J.* **2019,** *363*, 107-119.

(16) Karimi-Maleh, H.; Ayati, A.; Ghanbari, S.; Orooji, Y.; Tanhaei, B.; Karimi, F.; Alizadeh, M.; Rouhi, J.; Fu, L.; Sillanpää, M. Recent Advances in Removal Techniques of Cr(VI) Toxic Ion from Aqueous Solution: A Comprehensive Review. *J. Mol. Liq.* **2021,** *329*, 115062.

(17) Kong, X.; Ge, R.; Liu, T.; Xu, S.; Hao, P.; Zhao, X.; Li, Z.; Lei, X.;Duan, H., Super-Stable Mineralization of Cadmium by Calcium-Aluminum Layered Double Hydroxide and Its Large-Scale Application in Agriculture Soil Remediation. *Chem. Eng. J.* **2021,** *407*, 127178-127185.

(18) Xie, B.; Shan, C.; Xu, Z.; Li, X.; Zhang, X.; Chen, J.; Pan, B., One-Step Removal of Cr(VI) at Alkaline pH by UV/Sulfite Process: Reduction to Cr(III) and in Situ Cr(III) Precipitation. *Chem. Eng. J.* **2017,** *308*, 791-797.

(19) Zhou, J.-Z.; Wu, Y.-Y.; Liu, C.; Orpe, A.; Liu, Q.; Xu, Z.-P.; Qian, G.-R.; Qiao, S.-Z., Effective Self-Purification of Polynary Metal Electroplating Wastewaters through Formation of Layered Double Hydroxides. *Environ. Sci. Technol.* **2010,** *44*, 8884-8890.

(20) Ma, L.; Islam, S. M.; Xiao, C.; Zhao, J.; Liu, H.; Yuan, M.; Sun, G.; Li, H.; Ma, S.; Kanatzidis, M. G., Rapid Simultaneous Removal of Toxic Anions $[HSeO_3]^-$, $[SeO_3]^{2-}$, and $[SeO_4]^{2-}$, and Metals Hg^{2+}, Cu^{2+}, and Cd^{2+} by MoS_4^{2-} Intercalated Layered Double Hydroxide. *J. Am. Chem. Soc.* **2017,** *139*, 12745-

12757.

(21) Chambonneau, M.; Grojo, D.; Tokel, O.; Ilday, F. Ö.; Tzortzakis, S.; Nolte, S., In-Volume Laser Direct Writing of Silicon—Challenges and Opportunities. *Laser Photonics Rev.* **2021,** *15*, 2100140-2100174.

(22) Li, P.; Huang, Y.; Fu, C.; Jiang, S. X.; Peng, W.; Jia, Y.; Peng, H.; Zhang, P.; Manzie, N.; Mitter, N.; Xu, Z. P., Eco-Friendly Biomolecule-Nanomaterial Hybrids as Next-Generation Agrochemicals for Topical Delivery. *EcoMat.* **2021,** *3*, e12132.

(23) Parbrook, P. J.; Corbett, B.; Han, J.; Seong, T.-Y.; Amano, H., Micro-Light Emitting Diode: From Chips to Applications. *Laser Photonics Rev.* **2021,** *15*, 2000133.

(24) Popkova, A. A.; Antropov, I. M.; Tselikov, G. I.; Ermolaev, G. A.; Ozerov, I.; Kirtaev, R. V.; Novikov, S. M.; Evlyukhin, A. B.; Arsenin, A. V.; Bessonov, V. O.; Volkov, V. S.;Fedyanin, A. A., Nonlinear Exciton-Mie Coupling in Transition Metal Dichalcogenide Nanoresonators. *Laser Photonics Rev.* **2022,** *16*, 2100604.

(25) Zhang, S.; Han, B.; Zhang, Y.-n.; Liu, Y.; Zheng, W.; Zhao, Y., Multichannel Fiber Optic Spr Sensors: Realization Methods, Application Status, and Future Prospects. *Laser Photonics Rev.* **2022,** 2200009.

(26) Chi, H.; Wang, J.; Wang, H.; Li, S.; Yang, M.; Bai, S.; Li, C.; Sun, X.; Zhao, Y.;Song, Y.-F., Super-Stable Mineralization of Ni^{2+} Ions from Wastewater Using Cafe Layered Double Hydroxide. *Adv. Funct. Mater.* **2021**, 2106645.

(27) Li, J.; Xu, Y.; Ding, Z.; Mahadi, A. H.; Zhao, Y.; Song, Y.-F., Photocatalytic Selective Oxidation of Benzene to Phenol in Water over Layered Double Hydroxide: A Thermodynamic and Kinetic Perspective. *Chem. Eng. J.* **2020,** *388*, 124248-124255.

(28) Ma, X.; Xu, Y.; Tan, L.; Zhao, Y.; Song, Y.-F., Visible-Light-Induced Hydrogenation of C=C Bonds by Hydrazine over Ultrathin Layered Double Hydroxide Nanosheets. *Ind. Eng. Chem. Res.* **2020,** *59*, 14315-14322.

(29) Wang, Z.; Xu, S.-M.; Xu, Y.; Tan, L.; Wang, X.; Zhao, Y.; Duan, H.; Song, Y.-F., Single Ru Atoms with Precise Coordination on a Monolayer Layered Double Hydroxide for Efficient Electrooxidation Catalysis. *Chem. Sci.* **2019,** *10*, 378-384.

(30) Zhang, F.; Zhang, Y.; Yue, C.; Zhang, R.; Yang, Y., Facile Fabrication of Spherical Architecture

of Ni/Al Layered Double Hydroxide Based Onin Situtransformation Mechanism. *AIChE J.* **2014,** *60*, 4027-4036.

(31) Yang, P.; Li, S.; Liu, C.; Liu, X., Interface-Constrained Layered Double Hydroxides for Stable Uranium Capture in Highly Acidic Industrial Wastewater. *ACS Appl. Mater. Inter.* **2021,** *13*, 17988-17997.

(32) Zhao, S.; Meng, Z.; Fan, X.; Jing, R.; Yang, J.; Shao, Y.; Liu, X.; Wu, M.; Zhang, Q.; Liu, A., Removal of Heavy Metals from Soil by Vermiculite Supported Layered Double Hydroxides with Three-Dimensional Hierarchical Structure. *Chem. Eng. J.* **2020,** *390*, 124554.

(33) Ma, L.; Islam, S. M.; Liu, H.; Zhao, J.; Sun, G.; Li, H.; Ma, S.; Kanatzidis, M. G., Selective and Efficient Removal of Toxic Oxoanions of As(III), As(V), and Cr(VI) by Layered Double Hydroxide Intercalated with MoS_4^{2-}. *Chem. Mater.* **2017,** *29*, 3274-3284.

(34) Lv, L.; He, J.; Wei, M.; Duan, X., Kinetic Studies on Fluoride Removal by Calcined Layered Double Hydroxides. *Ind. Eng. Chem. Res.* **2006,** *45*, 8623-8628.

(35) Kong, X.; Hao, P.; Duan, H., Super-Stable Mineralization Effect of Layered Double Hydroxides for Heavymetals: Application in Soil Remediation and Perspective. *Exploration* **2021,** *1*, 20210052.

(36) Zhu, S.; Chen, Y.; Khan, M. A.; Xu, H.; Wang, F.; Xia, M., In-Depth Study of Heavy Metal Removal by an Etidronic Acid-Functionalized Layered Double Hydroxide. *ACS Appl. Mater. Inter.* **2022,** *14*, 7450-7463.

(37) Boclair, J. W.; Braterman, P. S.; Jiang, J.; Lou, S.; Yarberry, F., Layered Double Hydroxide Stability. 2. Formation of Cr(III)-Containing Layered Double Hydroxides Directly from Solution. *Chem. Mater.* **1999,** *11*, 303-307.

(38) Boehm, H.-P.; Steinle, J.; Vieweger, C., $[Zn_2Cr(OH)_6]X.2H_2O$, New Layer Compounds Cap Able of Anion Exchange and Intracrystalline Swelling. *Angew. Chem. Int. Ed.* **1977,** *16*, 265-266.

(39) Williams, G. R.; Clout, A.; Burley, J. C., A Kinetic and Mechanistic Study into the Formation of the Cu-Cr Layered Double Hydroxide. *Phys. Chem. Chem. Phys.* **2013,** *15*, 8616-8628.

(40) Williams, G. R.; O'Hare, D., A Kinetic Study of the Intercalation of Lithium Salts into $Al(OH)_3$. *J. Phys. Chem. B* **2006,** *110*, 10619-10629.

(41) Siavash Moakhar, R.; Hosseini-Hosseinabad, S. M.; Masudy-Panah, S.; Seza, A.; Jalali, M.; Fallah-Arani, H.; Dabir, F.; Gholipour, S.; Abdi, Y.; Bagheri-Hariri, M.; Riahi-Noori, N.; Lim, Y.-F.;

Hagfeldt, A.; Saliba, M., Photoelectrochemical Water-Splitting Using Cuo-Based Electrodes for Hydrogen Production: A Review. *Adv. Mater.* **2021,** *33*, 2007285.

(42) Yan, X.; Kang, H.; Cheng, P.; Zhang, S.; Shi, S.;Liu, W., Monolithic Three-Dimensional Hollow Nanoporous Cu_xO Encapsulated Mesoporous Cu Heterostructures with Superior Li Storage Properties. *EcoMat.* **2022,** e12208.

(43) You, Y.; Huang, H.; Mao, K. K.; Xia, S.; Wu, D.; Hu, C. Y.; Gao, C.; Liu, P. Y. M.; Long, R.; Wu, X. J.; Xiong, Y. J., Tandem Nanocatalyst Design: Putting Two Step-Reaction Sites into One Location Towards Enhanced Hydrogen Transfer Reactions. *Sci. China Mater.* **2019,** *62*, 1297-1305.

(44) Tao, X. Q.; Long, R.; Wu, D.; Hu, Y. G.; Qiu, G. H.; Qi, Z. M.; Li, B. X.; Jiang, R. B.; Xiong, Y. J., Anchoring Positively Charged Pd Single Atoms in Ordered Porous Ceria to Boost Catalytic Activity and Stability in Suzuki Coupling Reactions. *Small* **2020,** *16*, 2001782.

(45) Zhou, J.; Liu, X.; Zheng, J.; Li, L.; Liu, W.; Lin, L.; Lin, Z., Simultaneous Separation and Immobilization of Cr(VI) from Layered Double Hydroxide Via Reconstruction of the Key Phases. *J. Hazard. Mater.* **2021,** *416*, 125807.

(46) Zhang, Y.; Xu, X.; Yue, C.; Song, L.; Lv, Y.; Liu, F.;Li, A. Insight into the Efficient Co-Removal of Cr(VI) and Cr(III) by Positively Charged UiO-66-NH_2 Decorated Ultrafiltration Membrane. *Chem. Eng. J.* **2021,** *404*, 126546.

(47) Zhao, Y.; Zhao, Y.; Waterhouse, G. I. N.; Zheng, L.; Cao, X.; Teng, F.; Wu, L.-Z.; Tung, C.-H.; O'Hare, D.; Zhang, T., Layered-Double-Hydroxide Nanosheets as Efficient Visible-Light-Driven Photocatalysts for Dinitrogen Fixation. *Adv. Mater.* **2017,** *29*, 1703828.

(48) Wang, Y.; Zhao, Y.; Liu, J.; Li, Z.; Waterhouse, G. I. N.; Shi, R.; Wen, X.; Zhang, T., Manganese Oxide Modified Nickel Catalysts for Photothermal Co Hydrogenation to Light Olefins. *Adv. Energy Mater.* **2019,** *10*, 1902860.

(49) Xue, Q.; Xie, Y.; Wu, S.; Wu, T. S.; Soo, Y. L.; Day, S.; Tang, C. C.; Man, H. W.; Yuen, S. T.; Wong, K. Y.; Wang, Y.; Lo, B. T. W.; Tsang, S. C. E., A Rational Study on the Geometric and Electronic Properties of Single-Atom Catalysts for Enhanced Catalytic Performance. *Nanoscale* **2020,** *12*, 23206-23212.

(50) Wang, Z.; Xu, S.-M.; Tan, L.; Liu, G.; Shen, T.; Yu, C.; Wang, H.; Tao, Y.; Cao, X.; Zhao, Y.; Song, Y.-F., 600 Nm-Driven Photoreduction of CO_2 through the Topological Transformation of Layered

Double Hydroxides Nanosheets. *Appl. Catal. B Environ.* **2020,** *274*, 118884.

(51) Irie, H.; Kamiya, K.; Shibanuma, T.; Miura, S.; Tryk, D. A.; Yokoyama, T.;Hashimoto, K., Visible Light-Sensitive Cu(II)-Grafted TiO_2 Photocatalysts: Activities and X-Ray Absorption Fine Structure Analyses. *J. Phys. Chem. C* **2009,** *113*, 10761-10766.

(52) Abe, H.; Niwa, Y.; Kimura, M.; Murakami, Y.; Yokoyama, T.;Hosono, H. Gritty Surface Sample Holder Invented to Obtain Correct X-Ray Absorption Fine Structure Spectra for Concentrated Materials by Fluorescence Yield. *Anal. Chem.* **2016,** *88*, 3455-3458.

(53) Li, B.; Zhang, Y.; Zhou, X.; Liu, Z.; Liu, Q.; Li, X., Different Dye Removal Mechanisms between Monodispersed and Uniform Hexagonal Thin Plate-Like MgAl–CO_3^{2-}-LDH and Its Calcined Product in Efficient Removal of Congo Red from Water. *J. Alloy. Compd.* **2016,** *673*, 265-271.

(54) Chen S.; Huang Y.; Han X.; Wu Z.; Lai C.; Wang J.; Deng Q.; Zeng Z.; Deng S., Simultaneous and Efficient Removal of Cr(VI) and Methyl Orange on Ldhs Decorated Porous Carbons. *Chem. Eng. J.* **2018,** *352*, 306-315.

(55) Gao, H.; Cao, R.; Xu, X.; Xue, J.; Zhang, S.; Hayat, T.; Alharbi, N. S.; Li, J. Surface Area- and Structure-Dependent Effects of LDH for Highly Efficient Dye Removal. *ACS Sustain. Chem. Eng.* **2019,** *7*, 905-915.

(56) Wang, Q.; Wang, X.; Shi, C., LDH Nanoflower Lantern Derived from ZIF-67 and Its Application for Adsorptive Removal of Organics from Water. *Ind. Eng. Chem. Res.* **2018,** *57*, 12478-12484.

(57) Wang, X.; Cheng, B.; Zhang, L.; Yu, J.; Li, Y., Synthesis of MgNiCo LDH Hollow Structure Derived from ZIF-67 as Superb Adsorbent for Congo Red. *J. Colloid Interf. Sci.* **2022,** *612*, 598-607.

(58) Sriram, G.; Uthappa, U. T.; Losic, D.; Kigga, M.; Jung, H.-Y.; Kurkuri, M. D., Mg-Al-Layered Double Hydroxide (LDH) Modified Diatoms for Highly Efficient Removal of Congo Red from Aqueous Solution. *Appl. Sci.* **2020,** *10*, 2285-2303.

(59) Zhao, Y.; Waterhouse, G. I. N.; Chen, G.; Xiong, X.; Wu, L.-Z.; Tung, C.-H.; Zhang, T., Two-Dimensional-Related Catalytic Materials for Solar-Driven Conversion of CO_x into Valuable Chemical Feedstocks. *Chem. Soc. Rev.* **2019,** *48*, 1972-2010.

(60) Zhang, Z.; Ding, X.; Yang, X.; Tu, W.; Wang, L.; Zou, Z., Shedding Light on CO_2: Catalytic Synthesis of Solar Methanol. *EcoMat.* **2021,** *3*, e12078.

(61) Tan, L.; Xu, S.-M.; Wang, Z.; Xu, Y.; Wang, X.; Hao, X.; Bai, S.; Ning, C.; Wang, Y.; Zhang, W.; Jo, Y.-K.; Hwang, S.-J.; Cao, X.; Zheng, X.; Yan, H.; Zhao, Y.;Duan, H.; Song, Y.-F., Highly Selective Photoreduction of CO_2 with Suppressing H_2 Evolution over Monolayer Layered Double Hydroxide under Irradiation above 600 Nm. *Angew. Chem. Int. Ed.* **2019,** *58*, 11860-11867.

(62) Luo, Y.; Wu, Y.; Huang, C.; Menon, C.; Feng, S.-P.; Chu, P. K., Plasma Modified and Tailored Defective Electrocatalysts for Water Electrolysis and Hydrogen Fuel Cells. *EcoMat.* **2022,** *4*, e12197.

(63) Bai, S.; Li, T.; Wang, H.; Tan, L.; Zhao, Y.; Song, Y.-F., Scale-up Synthesis of Monolayer Layered Double Hydroxide Nanosheets Via Separate Nucleation and Aging Steps Method for Efficient CO_2 Photoreduction. *Chem. Eng. J.* **2021,** *419*, 129390-129398.

(64) Ning, C.; Wang, Z.; Bai, S.; Tan, L.; Dong, H.; Xu, Y.; Hao, X.; Shen, T.; Zhao, J.; Zhao, P.; Li, Z.; Zhao, Y.; Song, Y.-F., 650 nm-Driven Syngas Evolution from Photocatalytic CO_2 Reduction over Co-Containing Ternary Layered Double Hydroxide Nanosheets. *Chem. Eng. J.* **2021,** *412*, 128362.

(65) Teramura, K.; Iguchi, S.; Mizuno, Y.; Shishido, T.; Tanaka, T. Photocatalytic Conversion of CO_2 in Water over Layered Double Hydroxides. *Angew. Chem., Int. Ed.* **2012,** *51*, 8008-8011.

(66) Wang, Y.; Huang, N.-Y.; Shen, J.-Q.; Liao, P.-Q.; Chen, X.-M.; Zhang, J.-P. Hydroxide Ligands Cooperate with Catalytic Centers in Metal–Organic Frameworks for Efficient Photocatalytic CO_2 Reduction. *J. Am. Chem. Soc.* **2018,** *140*, 38-41.

(67) Jiao, F.; Li, J.; Pan, X.; Xiao, J.; Li, H.; Ma, H.; Wei, M.; Pan, Y.; Zhou, Z.; Li, M.; Miao, S.; Li, J.; Zhu, Y.; Xiao, D.; He, T.; Yang, J.; Qi, F.; Fu, Q.; Bao, X., Selective Conversion of Syngas to Light Olefins. *Science* **2016,** *351*, 1065-1068.

(68) Albero, J.; Peng, Y.; García, H., Photocatalytic CO_2 Reduction to C2+ Products. *ACS Catal.* **2020,** *10*, 5734-5749.

For Table of Contents Only

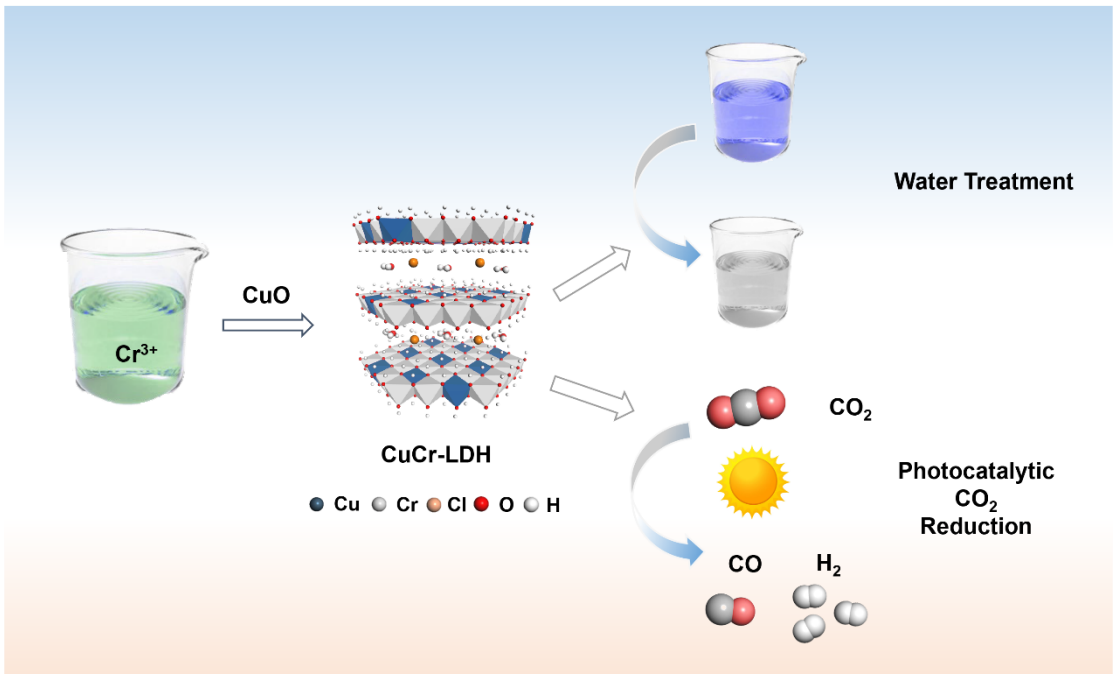

We report herein a super-stable mineralization method to immobilize Cr^{3+} ions from wastewater using CuO as a stabilizer, leading to the formation of CuCr-LDH, which can be used to remove organic dyes and photocatalytic CO_2 reduction.